Thermodynamic cost of a shortcuts-to-isothermal transport of a Brownian particle

John A. C. Albay,[1] Sarah R. Wulaningrum,[1] Chulan Kwon,[2] Pik-Yin Lai,[1,*] and Yonggun Jun[1,†]
[1]*Department of Physics, National Central University, Chung-Li District, Taoyuan City 320, Taiwan*
[2]*Department of Physics, Myongji University, Yongin, Gyeonggi-do 17058, Korea*

(Received 15 July 2019; published 22 November 2019)

We study the thermodynamic energy cost required for the shortcuts-to-isothermal (ScI) process that can accelerate the isothermal process at a finite time. Our experiment uses a Brownian particle dragged by the harmonic potential between two equilibrium positions with free energy difference. We confirm theoretically and experimentally that the probability distribution functions of work done during these processes are Gaussian, and the dissipated work for ScI transport is inversely proportional to the driving time, indicating that very prompt transition is impossible because of a diverging driving cost.

DOI: 10.1103/PhysRevResearch.1.033122

An isothermal process is a cornerstone in classical thermodynamics, whose transition from one equilibrium state to another takes a very long time to be completed [1]. Thanks to the recent technical advances in manipulating nanosize objects, such as optical tweezers [2], magnetic tweezers [3], and the Anti-Brownian ELectrokinetic (ABEL) trap [4], there has been more focus on understanding small systems where thermal fluctuations are dominant [5]. In particular, the realization of the Brownian heat engine has refocused attention on thermodynamic processes in stochastic thermodynamics [6,7]. One obvious question is whether it is possible to accelerate a system from one equilibrium state to another with a time much shorter than the intrinsic relaxation time and thus reproduce the same output as in a quasistatic process. For the past decade, there have been many studies in quantum systems, known as shortcuts to adiabaticity [8–14], as well as in stochastic environments [15–18]. These shortcuts require extra energy to suppress highly nonequilibrium fluctuations. However, the thermodynamic cost to boost such fast isothermal transitions has not been experimentally explored. In particular, the recently proposed shortcuts-to-isothermality (ScI) [17] method provided a unified framework to realize the finite-rate isothermal process and determine nonequilibrium work relations. Accelerated isothermal process is of both fundamental and practical importance in realizing thermodynamic cycles in microheat engines and ScI can speed up significantly the engine cycle. Understanding the associated cost for ScI processes is critical to improving the efficiency in the design of such microengines.

In this paper, we experimentally demonstrate the finite-time isothermal transport of a Brownian particle dragged by the harmonic potential between two equilibrium states with free energy difference ΔF to examine the thermodynamic cost to accelerate the isothermal process. For realization, the laser center is shifted by the acousto-optic deflector (AOD) at the rate of 100 kHz according to the ScI protocol proposed. We measure the work done during transport and compare its distribution to the Gaussian work distribution function derived from the moment of work distribution [19]. We obtain the thermodynamic energy cost for ScI protocol that is inversely proportional to the driving time, indicating that prompt transition is impossible due to the infinite cost.

The fundamental idea to experimentally realize the ScI transport of a Brownian particle is depicted in Fig. 1. Let us consider a particle trapped in a one-dimensional time-dependent harmonic potential $U_0(x,t) = kx^2/2 - \lambda(t)x$ at temperature T, where x is the particle displacement from the initial position of the potential center, k is the stiffness of the potential, and $\lambda(t)$ is the external dragging force turned on at $t = 0$. Note that the detailed derivation for the general case is given in Appendix B. The protocol performing with U_0 is called the RAMP protocol because the laser position monotonically increases in contrast to the ScI protocol. The motion of the particle can be described by the overdamped Langevin equation,

$$-\gamma\dot{x}(t) + f_0(x,t) + \xi^f(t) = 0, \tag{1}$$

where $\gamma = 6\pi\eta R$ is the drag coefficient, η is the viscosity of the surrounding medium, R is the radius of the particle, and the force $f_0(x,t) = -\partial U_0(x,t)/\partial x$. $\xi^f(x,t)$ is the random thermal force with zero mean and the variance $\langle \xi^f(t)\xi^f(t')\rangle = 2\gamma\delta(t-t')/\beta$ with the inverse temperature, $\beta = 1/k_BT$, and the Boltzmann constant k_B.

In the ScI protocol, it is hypothesized that the distribution function is invariant during transport, indicating instantaneous equilibrium (ieq) of the transition,

$$\rho(x,t) = \rho_{\rm ieq}(x,\lambda(t)) \propto e^{-\beta U_0(x,t)} = e^{-\frac{\beta k}{2}(x-\bar{x}(t))^2}, \tag{2}$$

where $\bar{x}(t)$ is the mean position of the particle at the given time. To maintain the evolution of the system always in instantaneous equilibrium with the RAMP potential U_0, an auxiliary potential $U_{\rm aux}(x,t)$ is introduced to the system

*pylai@phy.ncu.edu.tw
†yonggun@phy.ncu.edu.tw

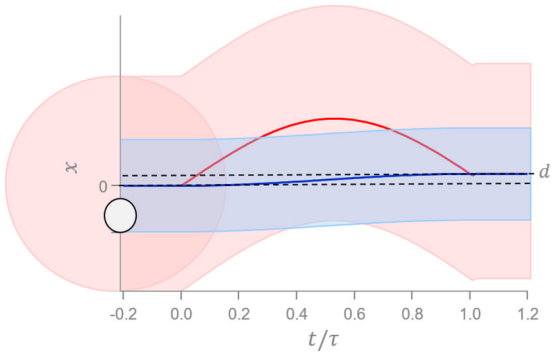

FIG. 1. The illustration of ScI transport of a Brownian particle by the harmonic potential. The laser spot (red circle) moves along the red line and the trapped particle is expected to fluctuate centered at the expected mean path (blue line). At $t < 0$, the particle stays at the equilibrium position $\langle x_i \rangle$. When the protocol is turned on, the particle is dragged by the harmonic potential to another equilibrium position x_f. For $t > \tau$, it stays at $\langle x_f \rangle = d$, where τ is the driving time.

such that the joint potential is $U(x, \lambda(t)) = U_0(x, \lambda(t)) + U_{\text{aux}}(x, t)$. The analytic form for the auxiliary potential for the given potential is given as $U_{\text{aux}}(x, t) = -\gamma\dot{\lambda}(t)/kx$ [17]. Eventually, the form of the potential for the ScI protocol becomes

$$U(x, \lambda(t)) = \frac{1}{2}kx^2 - \lambda(t)x - \frac{\gamma\dot{\lambda}(t)}{k}x. \tag{3}$$

The boundary conditions for U_{aux} have to be $\dot{\lambda}(0) = \dot{\lambda}(\tau) = 0$ because the auxiliary potential must be applied only during the process and thus the joint potential must be U_0 at $t = 0$ and $t = \tau$. Theoretical results are derived for general protocol $\lambda(t)$ as given in Appendix B. In the experiments, we choose the following form of the auxiliary force satisfying the boundary conditions,

$$\lambda(t) = a\left[1 - \cos\left(\frac{\pi t}{\tau}\right)\right]k\sigma, \tag{4}$$

where a is the strength of the auxiliary force, $\sigma = \sqrt{1/k\beta}$ is the width of the particle fluctuation in the harmonic potential, and τ is the transport time from one equilibrium state to another. In Fig. 1, the red circle indicates the linear range of the optical tweezers where the particle (the white circle) must be within during whole process, or otherwise the particle would experience a different force. At $t = 0$, the protocol is turned on, and the particle starts to be dragged by the moving potential from initial equilibrium state, $\langle x_i \rangle = 0$ to final equilibrium state, $\langle x_f \rangle = d$, with $x_{lc} = \lambda/k$ for the RAMP protocol and $x_{lc} = \lambda/k + \dot{\lambda}\gamma/k^2$ for the ScI counterpart, where x_{lc} is the laser center position. Because the laser (red solid line) moves far from the mean particle trajectory (blue solid line) for the ScI transport, the optical tweezers apply a stronger dragging force on the particle than they do for the RAMP protocol and so maintain instantaneous equilibrium during the transition process.

The details of the experimental setup are described in our previously published work [20,21]. The optical tweezers system has one limitation to achieve the ScI transport at the short transport time. As shown in Fig. 1, the blue solid line is the expected mean position of the particle for the ScI process. Because the particle fluctuations (blue shadow) must stay inside the linear range (red shadow) of the optical tweezers during the whole process, the laser center cannot move far away from the expected mean particle position. Thus, the optimal experimental condition is as follows: The stiffness is $k = 3.6 \pm 0.1\,\text{pN}/\mu\text{m}$, the corresponding intrinsic relaxation time is $\tau_c = 2.6\,\text{ms}$, and the minimum processing time is $\tau = 1\,\text{ms}$. While under this condition, the transport distance of a particle is 25 nm, much smaller than the particle diameter of 1 μm, and our measurement captures most of important physics of finite-rate isothermal process as described below.

The experiments have three steps: (i) The particle fluctuates in the harmonic potential for 50 ms for the initial equilibrium state. (ii) Two protocols for transport are realized to be compared. The first protocol is the RAMP transport processed by $U_0(x, t)$ to look into the intrinsic relaxation of the system. Second is the ScI protocol, not only done with the same experimental parameters with the RAMP but also with the additional auxiliary potential $U_{\text{aux}}(x, t)$. The RAMP and ScI transport were realized at various process times of $\tau = 1$, 2, 3, 10, 25, 50, and 75 ms. (iii) The potential stays for 50 ms to wait for the particle to return to the another equilibrium state. Then, the potential moves back to the initial position. For each transport time, the measurements of both protocols are repeated for 12 000 cycles.

Figure 2(a) presents the color maps of the time evolution of position histogram of the particle driven by the RAMP (left) and ScI (right) protocol at the process time of 1 ms. Here, the white line indicates the mean particle trajectory, the pink is the trajectory of the quasistatic isothermal process, and the black line is the harmonic potential trajectory. When the protocols are turned on at $t = 0\,\text{ms}$, the laser moves sinusoidally from $x = 0$ to $2a\sigma$. For the RAMP protocol, the particle does not immediately follow the laser and returns to the equilibrium position after 20 ms. In contrast, for the ScI transport, the laser moves far away from the expected mean particle position to apply the auxiliary force that escorts the particle in equilibrium during the process. With ScI, the particle always follows the trajectory of the quasistatic isothermal process and thus achieves 20 times faster relaxation than the RAMP does. We also checked the basic hypothesis of the ScI [Eq. (2)] that the system is always at instantaneous equilibrium during the process, although the total system including the auxiliary potential is highly out of equilibrium. Thus, the histograms of the instantaneous particle position during the laser shift must collapse into the Boltzmann distribution in Eq. (2). Figure 2(b) shows that the measured instantaneous position histogram of the particle subtracted by the mean particle trajectory, $P(x - \bar{x})$, from the ScI transport. The colored dots represent the 300 individual histograms at different times ($-1\text{ms} < t < 2\text{ms}$) shown as the white box in Fig. 2(a). Our finding that all distributions collapse into a single Gaussian curve agrees well with the ScI assumption that the system evolves along the instantaneous equilibrium state of the initial potential.

In Fig. 3, the mean trajectories of the dragged particle for the RAMP and ScI protocol are compared for various values of τ. For each measurement, the stiffnesses of the harmonic potential and thus the corresponding characteristic lengths, σ,

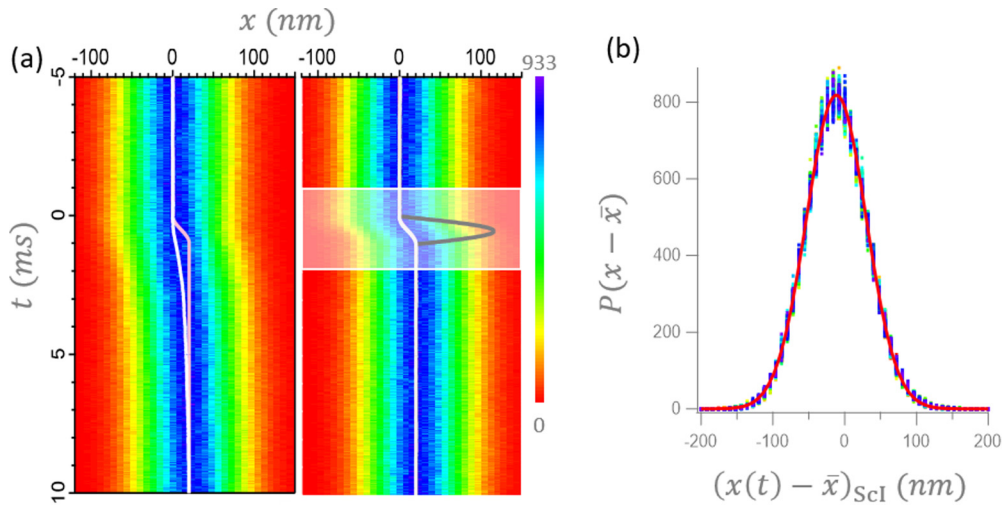

FIG. 2. (a) The color map of the time evolution of position histogram of the particle driven by the RAMP (left) and ScI (right) protocol at the process time of 1ms. Both protocols are turned on at t = 0 ms. The white and black lines indicate the particle and the laser center trajectories, respectively. (b) The instantaneous histograms of the particle position marked by the white box in panel (a) for 3 ms ($-1 < t < 2$ ms). The colored dots are the 300 individual histograms at different times, and the red solid line is the Gaussian distribution function. All histograms collapse into a single curve.

are not identical, so we rescaled the mean particle trajectories by the final equilibrium position, $x_{lc}(\tau) = 2a\sigma$. The mean positions for the RAMP (dashed gray) and ScI (solid color) protocols are

$$X_{\mathrm{RAMP}}(t) = a\sigma\left(1 - \frac{1}{1+\left(\frac{\pi\tau_c}{\tau}\right)^2}\left[\cos\frac{\pi t}{\tau} + \frac{\pi\tau_c}{\tau}\sin\frac{\pi t}{\tau} + \left(\frac{\pi\tau_c}{\tau}\right)^2 e^{-\frac{t}{\tau_c}}\right]\right), \tag{5}$$

$$X_{\mathrm{ScI}}(t) = a\sigma\left(1 - \cos\frac{\pi t}{\tau}\right). \tag{6}$$

For the short $\tau < 20$ ms, we observed that relaxation to final equilibrium state for the RAMP protocol takes 20 ms, while for the ScI transport the mean trajectories accord with the expected equilibrium trajectories and is the process is much faster than that for the RAMP protocol. For 1-ms transition time, the relaxation time for ScI is 1 ms, which is 20 times faster than that for the RAMP protocol. As τ increases, the difference between two mean trajectories decreases and for $\tau > 20$ ms, two trajectories overlap each other, indicating that the transition is close to the quasistatic process.

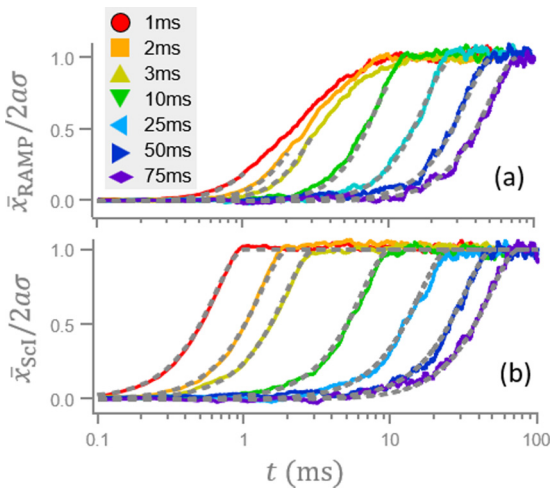

FIG. 3. The time evolution of the mean particle position for two distinct transport protocols: (a) RAMP and (b) ScI. The colors denote the different transport times τ and the gray dashed lines indicate the theoretical prediction of Eq. (5) for RAMP and Eq. (6) for ScI protocol.

Next, we turn our attention to the nonequilibrium work fluctuations during transport. The free energy difference between two equilibrium states is given by $\Delta F = \int_0^\tau dt\dot{\lambda}\frac{\partial U_0}{\partial\lambda} = -2a^2/\beta$. The measured work done during a single cycle of transport can be determined using the discretized Sekimoto formula $W = \int_0^\tau (\partial U/\partial t)dt$ [22]:

$$W_{\mathrm{RAMP}} = \Delta t\sum_i^N\left[-a\sin\left(\frac{\pi t_i}{\tau}\right)\frac{\pi k\sigma}{\tau}\right]x^{\mathrm{RAMP}}(t_i), \tag{7}$$

$$W_{\mathrm{ieq}} = \Delta t\sum_i^N\left[-a\sin\left(\frac{\pi t_i}{\tau}\right)\frac{\pi k\sigma}{\tau}\right]x^{\mathrm{ScI}}(t_i), \tag{8}$$

$$W_{\mathrm{ScI}} = W_{\mathrm{ieq}} + \Delta t\sum_i^N\left[-a\gamma\cos\left(\frac{\pi t_i}{\tau}\right)\frac{\pi^2\sigma}{\tau^2}\right]x^{\mathrm{ScI}}(t_i), \tag{9}$$

where the work from the RAMP process, the instantaneous equilibrium calculation, and the ScI are W_{RAMP}, W_{ieq}, and W_{ScI}, respectively. Here $N = \tau/\Delta t$, $\Delta t = 10\,\mu$s, $t_i = i\Delta t$ is the time step with $i = 0, 1, \ldots, N$.

Figure 4 shows the experimentally measured probability density functions (PDF) of the work done for various transport times τ (various symbols). The solid lines on the symbols are the fitting curves, and the vertical line indicates the free energy difference $\beta\Delta F = -0.125$. One notices that all PDFs for the three cases are well described by Gaussian distributions: $P(W) = 1/\sqrt{2\pi\sigma_W^2}\exp[-(W - \langle W\rangle)/2\sigma_W^2]$ (see the details in Appendix B). When the works are compared to the free energy difference ΔF, at $\tau < \tau_c$, the peaks for the RAMP

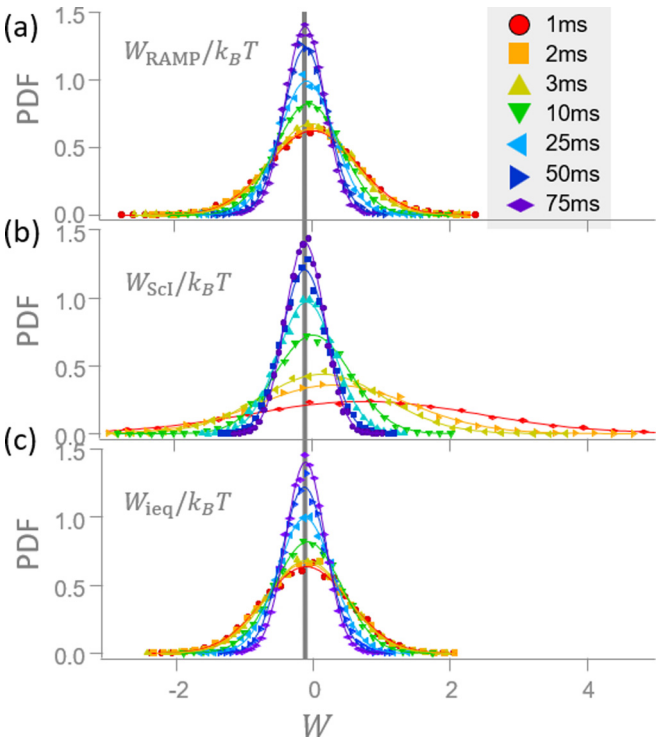

FIG. 4. The PDFs of work done for each transport cycle (a) for the RAMP protocol, W_{RAMP}; (b) for the ScI protocol, W_{ScI}, and (c) for the instantaneous work, W_{ieq}. The vertical line is the theoretical estimation of the free energy difference, ΔF.

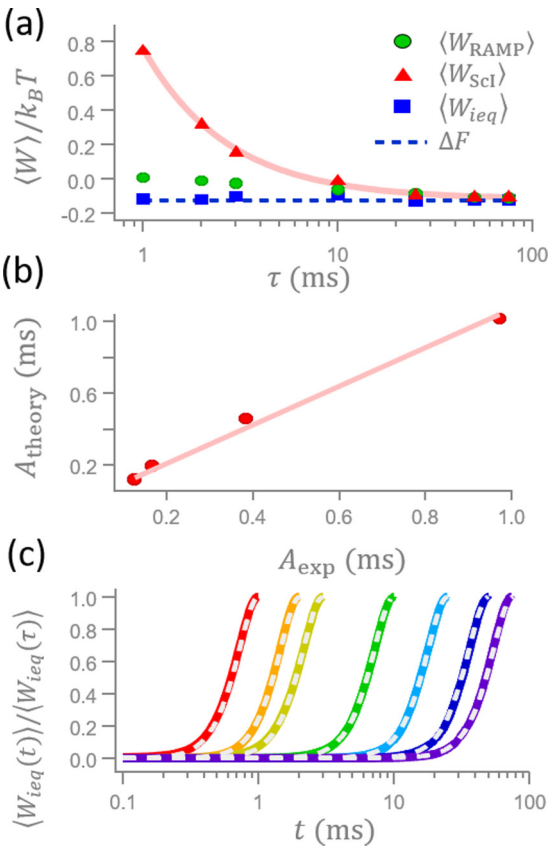

FIG. 5. (a) The averaged work from the RAMP (circles), ScI (squares), and ieq (triangles). The blue dashed line is the free energy difference from the theoretical calculation. (b) Comparison of the theoretical characteristic time, A_{theory}, to the experimental A_{exp} for the different τ_cs. (c) The instantaneous free energy difference normalized by $\langle W_{\mathrm{ieq}}(\tau)\rangle$ for the various values of τ.

protocol slightly deviate from ΔF and approach to ΔF as τ increases. For the ScI counterpart, the peak values are far from the ΔF and the width are broad for $\tau < \tau_c$, meaning that with ScI the process is highly nonequilibrium. For instantaneous equilibrium work W_{ieq}, all PDFs peak at ΔF over the whole transition time range. This ensures that the system driven by the ScI protocol behaves as if it is in equilibrium with the potential U_0 even though it is highly nonequilibrium.

Figure 5(a) shows the averaged work as a function of τ for the RAMP (circles), ScI (triangles), and ieq (squares). Here, the error bars are smaller than the symbol sizes. The averaged works for ScI, RAMP, and ieq processes are computed from (B26), (B28), (B30), and (B27) as

$$\beta\langle W_{\mathrm{ScI}}\rangle = \left(\frac{\pi^2}{2}\frac{\tau_c}{\tau} - 2\right)a^2, \tag{10}$$

$$\beta\langle W_{\mathrm{RAMP}}\rangle = \left(\frac{1+e^{-\tau/\tau_c}}{\left[1+\left(\frac{\tau}{\pi\tau_c}\right)^2\right]^2} + \frac{\tau/\tau_c}{2\left[1+\left(\frac{\tau}{\pi\tau_c}\right)^2\right]} - 2\right)a^2, \tag{11}$$

$$\beta\langle W_{\mathrm{ieq}}\rangle = -2a^2. \tag{12}$$

For the RAMP protocol, the work required to drag the particle is not far from the ΔF at short times and approaches to ΔF. For the ScI transport, as expected, the work to maintain the system in equilibrium with U_0 is much larger than that in the RAMP protocol. In other words, even when the total system is highly nonequilibrium with the ScI protocol, the particle stays in equilibrium with the RAMP protocol with extra work as the cost. The experimentally measured instantaneous work, $\beta\langle W_{\mathrm{ieq}}\rangle = -0.114 \pm 0.012$, clearly matches the theoretical calculation, $\beta\Delta F = -0.125$, and also confirms that during the transition it is always in equilibrium with the RAMP protocol. The solid curve in Fig. 5(a) is a fitting line of the thermodynamic cost to keep the particle in instantaneous equilibrium under ScI transport, which is the dissipated work and inversely proportional to the driving time, $\beta\langle W_{\mathrm{diss}}\rangle = \beta\langle W - \Delta F\rangle = A/\tau$, when the ScI transport is the optimal process [23]. This result also agrees well with the theoretical calculations [16,17]. For this specific protocol, the theoretical prediction (see Appendix C) gives $A_{\mathrm{theory}} = \pi^2 a^2 \tau_c/2 = 0.80$ ms, which is in agreement with the experimental value of 0.87 ± 0.01 ms. We performed more measurements with different τ_c to compare A_{exp} to the theoretical prediction. As shown in Fig. 5(b), the slope is close to 1. It is evident that the shorter driving time induces a larger driving cost and instantaneous jump to another equilibrium state is impossible due to the infinite cost.

We further characterize the property of the instantaneous equilibrium of the ScI transport in terms of the instantaneous free energy $\Delta F(t)$, which can be defined at the each moment of the process. That is theoretically simply given by $\beta\Delta F_{\mathrm{theo}}(t) = -\frac{a^2}{2}[1-\cos(\pi t/\tau)]^2$ and experimentally by $W_{\mathrm{ieq}}(t) \approx \frac{\Delta t}{M}\sum_{j=1}^{M}\sum_{i=1}^{t/\Delta t}(-a\sin(\pi t_i/\tau)\pi k\sigma/\tau)x_j^{\mathrm{ScI}}(t_i)$, where M is the number of the trajectories for averaging.

Figure 5(c) shows the measured instantaneous work normalized by that at the end of transition as a function of t. $W_{\rm ieq}(t)$ is represented by the solid line and $\Delta F_{\rm theo}(t)$ by the dashed line. The experimental results agree very well with the theoretical predictions, indicating that the particle behaves as if it is in equilibrium during the entire process.

To summarize, we experimentally realized the shortcuts-to-isothermal transport of a Brownian particle dragged by optical tweezers from one equilibrium state to another at finite times. We showed that although it takes 20 ms to relax to the equilibrium state at the fast shift of the potential with the RAMP protocol, the system can reach equilibrium 20 times faster with the escort of the auxiliary potential and that the position PDFs are invariant and Boltzmann during the transport. Also, we have computed the nonequilibrium work relation and showed it is accurately predicted by theoretical values. Work done to maintain the system in instantaneous equilibrium is much larger than that from the RAMP protocol and inversely scales with the processing time. Our results indicate that if a particle is driven with the shortcuts-to-isothermal protocol, it behaves as if it is in equilibrium although the system is governed by a highly nonequilibrium process.

Although the optical tweezers can be described by a harmonic potential in some regimes, to overcome practical issues and realize them in experiments require careful design and technical effort so that accurate measurements can be carried in appropriate timescales. Experimental realization of the theoretical results indicates that one actually can accelerate an isothermal process, with some cost. The experimental realization strongly suggests one can make use of ScI in designing microscale heat engines in practice.

We would like to thank Yung-Fu Chen and Bongsoo Kim for helpful discussions. This work was supported by the MoST of Taiwan under Grants No. 105-2112-M-008-026-MY3 (Y.J.) and No. 107-2112-M-008-003-MY3 (P.-Y.L.) and also by NRF Grant No. 2016R1D1A1A09918020 in Korea (C.K.).

APPENDIX A: INSTANTANEOUS EQUILIBRIUM POSITION DISTRIBUTION

Figure 6 shows the PDFs of time evolution of the measured particle position distribution in different process time τ. Figures 6(a)–6(c) are for faster processing times than the characteristic relaxation time τ_c while Figs. 6(d)–6(f) are for the slower processing times. The gray and black lines indicate the mean particle position and the movement of the laser center during the process, respectively. For $\tau < \tau_c$, the laser moves very far from the mean particle position, indicating the stronger dragging force applied to the particle during the process. This auxiliary force by the laser keeps the distribution in instantaneous equilibrium with respect to the RAMP protocol. As τ becomes larger than τ_c, the transport is going to be the quasistatic process so that the laser center trajectories are very close to the center of the position distribution and thus the work done approaches ΔF, as shown in Fig. 5(a).

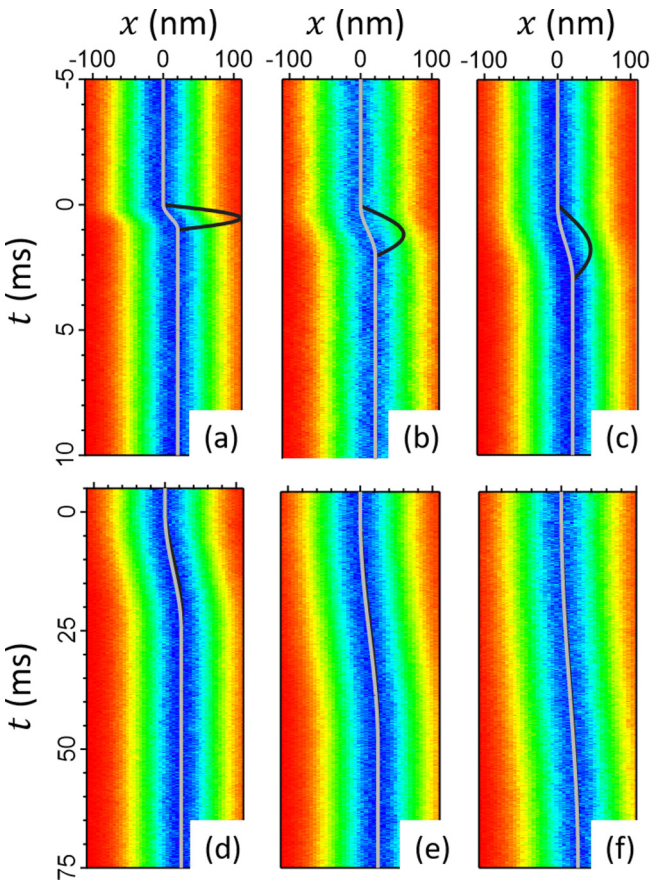

FIG. 6. The color map of the time evolution of position histogram of the particle driven by the ScI protocol at different processing time: (a) 1, (b) 2, (c) 3, (d) 25, (e) 50, and (f) 75 ms. All protocols are turned on at $t = 0$ ms. The gray and black lines indicate the mean particle and the laser center trajectories, respectively.

APPENDIX B: PARTICLE UNDER TIME-DEPENDENT HARMONIC POTENTIALS: RAMP AND SCI PROTOCOLS

Let us consider a particle trapped in a one-dimensional time-dependent harmonic potential of the form

$$U_{\rm RAMP}(x,t) = \tfrac{1}{2}kx^2 - \lambda(t)x. \tag{B1}$$

To maintain the evolution of the system always in instantaneous equilibrium with the original potential $U_{\rm RAMP}$, an auxiliary potential $U_{\rm aux}(x,t)$ is introduced to the system such that the joint potential is $U_{\rm ScI}(x,\lambda(t)) = U_{\rm RAMP}(x,\lambda(t)) + U_{\rm aux}(x,t)$. The analytic form for the auxiliary potential for the given potential is given as $U_{\rm aux}(x,t) = -\gamma\dot{\lambda}(t)x/k$ [17]. Here, the dot on a variable is the time derivative of that variable. Eventually, the form of the potential for the ScI protocol becomes

$$U_{\rm ScI}(x,\lambda(t)) = \frac{1}{2}kx^2 - \tilde{\lambda}(t)x, \quad \tilde{\lambda}(t) \equiv \lambda(t) + \frac{\gamma\dot{\lambda}(t)}{k}. \tag{B2}$$

To ensure the ScI protocol reduces smoothly to the RAMP potential at the beginning and end of the ScI process, the conditions $\dot{\lambda}(0) = \dot{\lambda}(\tau) = 0$ are imposed. Throughout this paper, we shall denote the ScI of the protocol $\lambda(t)$ by $\tilde{\lambda}(t)$.

To find the minimum of the potential for the ScI process, Eq. (B2) can be rewritten as

$$U_{\rm ScI}(x,t) = \frac{1}{2}k\left[x - \frac{\tilde{\lambda}(t)}{k}\right]^2 - \frac{1}{2}k\left(\frac{\tilde{\lambda}(t)}{k}\right)^2,$$

and hence the minimum potential, i.e., the center of the potential, is $\frac{\tilde{\lambda}(t)}{k}$. For the RAMP potential, simply put $\tilde{\lambda} \to \lambda$ in the above results for the ScI protocol.

The Langevin equation for the ScI protocol is

$$\dot{x}(t) = \frac{1}{\gamma}[-kx + \tilde{\lambda}(t)] + \xi(t) \tag{B3}$$

where γ is the drag coefficient and ξ is a zero-mean white noise with $\langle \xi(t)\xi(t')\rangle = (2k_BT/\gamma)\delta(t-t')$. It is convenient to separate the motion of the particle into a deterministic part, $X(t) \equiv \langle x(t)\rangle$, and a stochastic part, $z(t)$, with $x = X + z$, and (B3) becomes

$$\dot{X} = -\frac{k}{\gamma}X + \frac{1}{\gamma}\tilde{\lambda}(t), \tag{B4}$$

$$\dot{z} = -\frac{k}{\gamma}z + \xi(t), \tag{B5}$$

whose solutions are

$$X(t) = \frac{1}{\gamma}\int_0^t dt' e^{-\frac{k}{\gamma}(t-t')}\tilde{\lambda}(t') + X(0)e^{-\frac{k}{\gamma}t}, \tag{B6}$$

$$z(t) = \frac{1}{\gamma}\int_0^t dt' e^{-\frac{k}{\gamma}(t-t')}\xi(t') + z(0)e^{-\frac{k}{\gamma}t}. \tag{B7}$$

Inserting the expression of $\tilde{\lambda}(t)$ from (B2) into (B6) and integrating by parts, one has

$$X(t) = \frac{\lambda(t)}{k} + (X(0) - \frac{\lambda(0)}{k})e^{-\frac{k}{\gamma}t}. \tag{B8}$$

When we use the condition of the protocol that initially the system is at equilibrium in a harmonic well centered at $\lambda(0)/k$, $X(0) = \langle x(0)\rangle = \lambda(0)/k$ and hence $X(t) = \langle x(t)\rangle = \lambda(t)/k$. Furthermore, (B6) can be rewritten (integrating by parts) as

$$X(t) = \frac{\tilde{\lambda}(t)}{k} - \frac{1}{k}\int_0^t dt'\dot{\tilde{\lambda}}(t')e^{-\frac{k}{\gamma}(t-t')}. \tag{B9}$$

The RAMP trajectory can also be decomposed in a similar way into deterministic and fluctuating parts as $x(t) = X_{\rm RAMP} + z(t)$. The fluctuating dynamics is the same as (B5) and the solution of $X_{\rm RAMP}$ is

$$X_{\rm RAMP}(t) = \frac{1}{\gamma}\int_0^t dt'\lambda(t')e^{-\frac{k}{\gamma}(t-t')} + \frac{\lambda(0)}{k}e^{-\frac{k}{\gamma}t} \tag{B10}$$

$$= \frac{\lambda(t)}{k} - \frac{1}{k}\int_0^t dt'\dot{\lambda}(t')e^{-\frac{k}{\gamma}(t-t')}. \tag{B11}$$

Equation (B5) describes a Brownian particle in a harmonic potential under zero-mean Gaussian white noise and thus possesses an equilibrium Boltzmann distribution of $\sqrt{\frac{\beta k}{2\pi}}e^{-\frac{\beta k}{2}z^2}$ at all times since initial equilibrium; i.e., z is a zero-mean Gaussian stochastic variable with

$$\langle z(t)\rangle = 0, \quad \langle z(t)z(t')\rangle = \frac{1}{\beta k}e^{-\frac{k}{\gamma}|t-t'|}. \tag{B12}$$

$z(t)$ can be viewed as a Gaussian random variable with weak (exponentially decaying with correlation time $\tau_c \equiv \gamma/k$) correlations.

Using $z(t) = x(t) - X(t)$ and $X(t) = \lambda(t)/k$, one can verify directly that probability distribution of the instantaneous position $x(t)$ indeed obeys the equilibrium Boltzmann distribution:

$$\begin{aligned} P_{\rm ScI}(x(t),t) &= \sqrt{\frac{\beta k}{2\pi}}e^{-\frac{\beta k}{2}[x(t)-\frac{\lambda(t)}{k}]^2} \\ &= \sqrt{\frac{\beta k}{2\pi}}e^{-\beta[\frac{k}{2}x(t)^2-\lambda(t)x(t)]}e^{-\frac{\beta\lambda(t)^2}{2k}} \\ &= \frac{e^{-\beta[\frac{k}{2}x(t)^2-\lambda(t)x(t)]}}{\int dx e^{-\beta[\frac{k}{2}x^2-\lambda(t)x]}} \\ &= \frac{e^{-\beta U_{\rm RAMP}(x,t)}}{\int dx e^{-\beta U_{\rm RAMP}(x,t)}} \equiv \rho_{\rm ieq}(x(t),t). \end{aligned} \tag{B13}$$

On the other hand, when using (B11), the RAMP process will result in the distribution function

$$\begin{aligned} P_{\rm RAMP}(x(t),t) &= \sqrt{\frac{\beta k}{2\pi}}e^{-\frac{\beta k}{2}[x(t)-\frac{\lambda(t)}{k}+\frac{1}{k}\int_0^t dt'\dot{\lambda}(t')e^{-\frac{k}{\gamma}(t-t')}]^2} \\ &= \rho_{\rm ieq}(x(t),t)\exp\Bigg[-\beta k\delta X_{\rm RAMP}(t) \\ &\quad\times\left(\frac{1}{2}\delta X_{\rm RAMP}(t) + \frac{\lambda(t)}{k} - x(t)\right)\Bigg], \end{aligned} \tag{B14}$$

where $\delta X_{\rm RAMP}(t) \equiv X_{\rm RAMP}(t) - \frac{\lambda(t)}{k} = -\frac{1}{k}\int_0^t dt'\dot{\lambda}(t')e^{-\frac{k}{\gamma}(t-t')}$. It explicitly reveals the non-Boltzmann correction for the nonequilibrium RAMP process. Under the quasistatic condition of $\dot{\lambda} \to 0$, $P_{\rm RAMP} \to \rho_{\rm ieq}$, recovering the quasiequilibrium Boltzmann result.

1. Generating function and work distribution

The work rate of the ScI protocol is $\dot{W} = -\dot{\tilde{\lambda}}x$ and hence the work in the ScI process is

$$W = -\int_0^\tau dt\dot{\tilde{\lambda}}(t)[X(t) + z(t)]. \tag{B15}$$

The probability distribution of W can be computed using the generating function

$$\begin{aligned} g(\alpha) &\equiv \langle e^{-\alpha\beta W}\rangle; \\ P(W) &= \frac{1}{2\pi}\int d\alpha e^{i\alpha\beta W}g(i\alpha). \end{aligned} \tag{B16}$$

In particular, $P(W)$ is Gaussian if $g(\alpha)$ is quadratic in α with mean and variance given by

$$\langle W\rangle = -\frac{1}{\beta}\frac{\partial \ln g(\alpha)}{\partial\alpha}\bigg|_{\alpha=0}, \tag{B17}$$

$$\langle W^2\rangle - \langle W\rangle^2 = \frac{1}{\beta^2}\frac{\partial^2 \ln g(\alpha)}{\partial\alpha^2}\bigg|_{\alpha=0}. \tag{B18}$$

For ScI given by (B2), $g(\alpha)$ is calculated using (B9) and by cumulant expansion as follows:

$$g(\alpha) \equiv \langle e^{-\alpha\beta W}\rangle = \langle e^{\alpha\beta\int_0^\tau dt\dot{\tilde{\lambda}}(t)[X(t)+z(t)]}\rangle \tag{B19}$$

$$= e^{\frac{\alpha\beta}{k}\int_0^\tau dt\dot{\tilde{\lambda}}(t)\tilde{\lambda}(t)} e^{-\frac{\alpha\beta}{k}\int_0^\tau dt\dot{\tilde{\lambda}}(t)\int_0^t dt'\dot{\tilde{\lambda}}(t')e^{-\frac{k}{\gamma}(t-t')}} \times \langle e^{\alpha\beta\int_0^\tau dt\dot{\tilde{\lambda}}(t)z(t)}\rangle. \tag{B20}$$

Since $z(t)$ is a zero-mean Gaussian random variable, cumulant expansion gives

$$\langle e^{\alpha\beta\int_0^\tau dt\dot{\tilde{\lambda}}(t)z(t)}\rangle = e^{\frac{(\alpha\beta)^2}{2}\int_0^\tau dt\dot{\tilde{\lambda}}(t)\int_0^\tau dt'\dot{\tilde{\lambda}}(t')\langle z(t)z(t')\rangle}. \tag{B21}$$

Integrating by parts the exponent of the first factor in the right-hand side of (B20) and using (B12), one finally gets

$$-\ln g(\alpha) = \frac{\beta\alpha(1-\alpha)}{k}\int_0^\tau dt\dot{\tilde{\lambda}}(t) \times \int_0^t dt'\dot{\tilde{\lambda}}(t')e^{-\frac{k}{\gamma}(t-t')} + \alpha\beta\Delta F, \tag{B22}$$

$$\Delta F \equiv -\frac{1}{2k}[\tilde{\lambda}(\tau)^2 - \tilde{\lambda}(0)^2]. \tag{B23}$$

The double integral in (B22) can be further simplified to $\frac{\gamma}{k}\int_0^\tau dt\dot{\lambda}(t)^2$.

Then $\ln(g(\alpha))$ is quadratic in α and hence $P(W)$ is Gaussian with mean and variance

$$\langle W\rangle = \frac{\gamma}{k^2}\int_0^\tau dt\dot{\lambda}(t)^2 + \Delta F, \tag{B24}$$

$$\langle W^2\rangle - \langle W\rangle^2 = \frac{2\gamma}{\beta k^2}\int_0^\tau dt\dot{\lambda}(t)^2 = \frac{2}{\beta}(\langle W\rangle - \Delta F). \tag{B25}$$

One can also compute the mean work for ScI process directly using (B15):

$$\langle W_{\rm ScI}\rangle = -\frac{1}{k}\int_0^\tau dt\dot{\tilde{\lambda}}(t)\lambda(t) = -\frac{1}{2k}[\lambda(\tau)^2 - \lambda(0)^2] - \frac{\gamma}{k^2}\int_0^\tau dt\ddot{\lambda}(t)\lambda(t) \tag{B26}$$

$$= \Delta F + \frac{\gamma}{k^2}\int_0^\tau dt\dot{\lambda}(t)^2,$$

which agrees with (B24). The mean dissipated work in the ScI process is then

$$\langle W_{\rm diss}\rangle = \langle W_{\rm ScI}\rangle - \Delta F = \frac{\gamma}{k^2}\int_0^\tau dt\dot{\lambda}(t)^2. \tag{B27}$$

It is clearly seen that the dissipated work is inversely proportional to the driving time τ, which agrees with Schiemdl and Seifert [23]. Similarly, using $W_{\rm RAMP} = -\int_0^\tau dt\dot{\lambda}(t)[X_{\rm RAMP}(t) + z(t)]$ and $W_{\rm ieq} = -\int_0^\tau dt\dot{\lambda}(t)[X(t) + z(t)]$, it is easy to see that the distributions of both $W_{\rm RAMP}$ and $W_{\rm ieq}$ are Gaussians with means and variances given by

$$\langle W_{\rm RAMP}\rangle = \Delta F + \frac{1}{k}\int_0^\tau dt\dot{\lambda}(t)\int_0^t dt'\dot{\lambda}(t')e^{-\frac{k}{\gamma}(t-t')}, \tag{B28}$$

$$\langle W^2_{\rm RAMP}\rangle - \langle W_{\rm RAMP}\rangle^2 = \frac{2}{\beta}(\langle W_{\rm RAMP}\rangle - \Delta F), \tag{B29}$$

$$\langle W_{\rm ieq}\rangle = \Delta F, \tag{B30}$$

$$\langle W^2_{\rm ieq}\rangle - \langle W_{\rm ieq}\rangle^2 = \langle W^2_{\rm RAMP}\rangle - \langle W_{\rm RAMP}\rangle^2. \tag{B31}$$

2. Jarzynski equality

Since both $W_{\rm ScI}$ and $W_{\rm RAMP}$ are Gaussian distributed, cumulant expansion together with (B25) and (B29) gives

$$\langle e^{-\beta W}\rangle = e^{-\beta\langle W\rangle + \frac{\beta^2}{2}(\langle W^2\rangle - \langle W\rangle^2)} = e^{-\beta\Delta F}; \tag{B32}$$

i.e., the Jarzynski equality (Integral fluctuation theorem) holds for the both ScI and RAMP processes.

APPENDIX C: PROTOCOL $\lambda(t) = a[1 - \cos(\frac{\pi t}{\tau})]k\sigma$

In this experiment, the driving protocol is given as

$$\lambda(t) = a\left[1 - \cos\left(\frac{\pi t}{\tau}\right)\right]k\sigma, \tag{C1}$$

where $\sigma = \sqrt{k_BT/k}$. Then,

$$\dot{\lambda}(t) = (ak\sigma\pi/\tau)\sin(\pi t/\tau), \quad \ddot{\lambda}(t) = (ak\sigma\pi^2/\tau^2)\cos(\pi t/\tau,) \tag{C2}$$

$$\tilde{\lambda}(t) = (ak\sigma)\left[1 - \cos\frac{\pi t}{\tau} + \frac{\gamma\pi}{k\tau}\sin\frac{\pi t}{\tau}\right], \quad \dot{\tilde{\lambda}}(t) = (ak\sigma)\frac{\pi}{\tau}\left[\sin\frac{\pi t}{\tau} + \frac{\gamma\pi}{k\tau}\cos\frac{\pi t}{\tau}\right], \tag{C3}$$

$$\int_0^t dt'\dot{\lambda}(t')e^{-\frac{k}{\gamma}(t-t')} = ak\sigma\frac{\pi\tau_c}{\tau}\frac{1}{1+\left(\frac{\pi\tau_c}{\tau}\right)^2}\left(\sin\frac{\pi t}{\tau} - \frac{\pi\tau_c}{\tau} \times \cos\frac{\pi t}{\tau} + \frac{\pi\tau_c}{\tau}e^{-\frac{t}{\tau_c}}\right). \tag{C4}$$

Free energy difference ΔF for the ScI (and the RAMP) process from $t = 0$ to $t = \tau$ can be calculated from (B23) to give

$$\Delta F = -2a^2k_BT. \tag{C5}$$

The mean positions for the RAMP and ScI protocols are

$$X_{\rm RAMP}(t) = a\sigma\left(1 - \frac{1}{1+\left(\frac{\pi\tau_c}{\tau}\right)^2}\left[\cos\frac{\pi t}{\tau} + \frac{\pi\tau_c}{\tau}\sin\frac{\pi t}{\tau} + \left(\frac{\pi\tau_c}{\tau}\right)^2 e^{-\frac{t}{\tau_c}}\right]\right), \tag{C6}$$

$$X_{\rm ScI}(t) = a\sigma\left(1 - \cos\frac{\pi t}{\tau}\right). \tag{C7}$$

The mean works for ScI, RAMP, and ieq processes are computed from (B26), (B28), (B30), and (B27) as

$$\beta\langle W_{\rm ScI}\rangle = \left(\frac{\pi^2}{2}\frac{\tau_c}{\tau} - 2\right)a^2, \quad \tau_c \equiv \frac{\gamma}{k}, \tag{C8}$$

$$\beta\langle W_{\rm RAMP}\rangle = \left\{\frac{1+e^{-\tau/\tau_c}}{\left[1+\left(\frac{\tau}{\pi\tau_c}\right)^2\right]^2} + \frac{\tau/\tau_c}{2\left[1+\left(\frac{\tau}{\pi\tau_c}\right)^2\right]} - 2\right\}a^2, \tag{C9}$$

$$\beta\langle W_{\rm ieq}\rangle = -2a^2, \tag{C10}$$

$$\beta\langle W_{\rm diss}\rangle = \frac{\pi^2a^2}{2}\frac{\tau_c}{\tau}. \tag{C11}$$

The variances can be calculated directly from (B25), (B29), and (B31) in the previous section.

[1] D. V. Schroeder, *An Introduction to Thermal Physics*, 1st ed. (Pearson, San Francisco, CA, 2000).

[2] A Ashkin, J. M. Dziedzic, J. E. Bjorkholm, and S. Chu, Observation of a single-beam gradient force optical trap for dielectric particles, Opt. Lett. **11**, 288 (1986).

[3] C. Gosse and V. Croquette, Magnetic tweezers: Micromanipulation and force measurement at the molecular level, Biophys. J. **82**, 3314 (2002).

[4] A. E. Cohen and W. E. Moerner, Method for trapping and manipulating nanoscale objects in solution, Appl. Phys. Lett. **86**, 093109 (2005).

[5] U. Seifert, Stochastic thermodynamics, fluctuation theorems, and molecular machines, Rep. Prog. Phys. **75**, 126001 (2012).

[6] V. Blickle and C. Bechinger, Realization of a micrometre-sized stochastic heat engine, Nat. Phys. **8**, 143 (2011).

[7] I. A. Martínez, É. Roldán, L. Dinis, D. Petrov, J. M. R. Parrondo, and R. A. Rica, Brownian Carnot engine, Nat. Phys. **12**, 67 (2015).

[8] S. Ibáñez, X. Chen, E. Torrontegui, J. G. Muga, and A. Ruschhaupt, Multiple Schrödinger Pictures and Dynamics in Shortcuts to Adiabaticity, Phys. Rev. Lett. **109**, 100403 (2012).

[9] A. del Campo, Shortcuts to Adiabaticity by Counterdiabatic Driving, Phys. Rev. Lett. **111**, 100502 (2013).

[10] D. Guéry-Odelin and J. G. Muga, Transport in a harmonic trap: Shortcuts to adiabaticity and robust protocols, Phys. Rev. A **90**, 063425 (2014).

[11] S. Campbell and S. Deffner, Trade-Off Between Speed and Cost in Shortcuts to Adiabaticity, Phys. Rev. Lett. **118**, 100601 (2017).

[12] A. Walther, F. Ziesel, T. Ruster, S. T. Dawkins, K. Ott, M. Hettrich, K. Singer, F. Schmidt-Kaler, and U. Poschinger, Controlling Fast Transport of Cold Trapped ions, Phys. Rev. Lett. **109**, 080501 (2012).

[13] R. Bowler, J. Gaebler, Y. Lin, T. R. Tan, D. Hanneke, J. D. Jost, J. P. Home, D. Leibfried, and D. J. Wineland, Coherent Diabatic Ion Transport and Separation in a Multizone Trap Array, Phys. Rev. Lett. **109**, 080502 (2012).

[14] S. An, D. Lv, A. del Campo, and K. Kim, Shortcuts to adiabaticity by counterdiabatic driving for trapped-ion displacement in phase space, Nat. Commun. **7**, 12999 (2016).

[15] I. A. Martínez, A. Petrosyan, D. Guéry-Odelin, E. Trizac, and S. Ciliberto, Engineered swift equilibration of a Brownian particle, Nat. Phys. **12**, 843 (2016).

[16] A. Bravetti and D. Tapias, Thermodynamic cost for classical counterdiabatic driving, Phys. Rev. E **96**, 052107 (2017).

[17] G. Li, H. T. Quan, and Z. C. Tu, Shortcuts to isothermality and nonequilibrium work relations, Phys. Rev. E **96**, 012144 (2017).

[18] A. Patra and C. Jarzynski, Shortcuts to adiabaticity using flow fields, New J. Phys. **19**, 125009 (2017).

[19] C. Kwon, J. D. Noh, and H. Park, Work fluctuations in a time-dependent harmonic potential: Rigorous results beyond the overdamped limit, Phys. Rev. E **88**, 062102 (2013).

[20] Y. Jun, S. K. Tripathy, B. R. J. Narayanareddy, M. K. Mattson-Hoss, and S. P. Gross, Calibration of optical tweezers for in vivo force measurements: How do different approaches compare? Biophys. J. **107**, 1474 (2014).

[21] J. A. C. Albay, G. Paneru, H. K. Pak, and Y. Jun, Optical tweezers as a mathematically driven spatio-temporal potential generator, Opt. Express **26**, 29906 (2018).

[22] K. Sekimoto, Langevin equation and thermodynamics, Prog. Theor. Phys. Suppl. **130**, 17 (1998).

[23] T. Schmiedl and U. Seifert, Efficiency at maximum power: An analytically solvable model for stochastic heat engines, Europhys. Lett. **81**, 20003 (2008).